Cell, Vol. 84, 863–874, March 22, 1996, Copyright ©1996 by Cell Press

Crystal Structure and Mutational Analysis of the Human CDK2 Kinase Complex with Cell Cycle–Regulatory Protein CksHs1

Yves Bourne,*† Mark H. Watson,* Michael J. Hickey,* William Holmes,‡ Warren Rocque,‡ Steven I. Reed,* and John A. Tainer*
*Department of Molecular Biology
Scripps Research Institute
10666 North Torrey Pines Road
La Jolla, California 92037
‡Glaxo–Wellcome
5 Moore Drive
Research Triangle Park, North Carolina 27709

Summary

The 2.6 Å crystal structure for human cyclin-dependent kinase 2 (CDK2) in complex with CksHs1, a human homolog of essential yeast cell cycle–regulatory proteins suc1 and Cks1, reveals that CksHs1 binds via all four β strands to the kinase C-terminal lobe. This interface is biologically critical, based upon mutational analysis, but far from the CDK2 N-terminal lobe, cyclin, and regulatory phosphorylation sites. CDK2 binds the Cks single domain conformation and interacts with conserved hydrophobic residues plus His-60 and Glu-63 in their closed β-hinge motif conformation. The β hinge opening to form the Cks β-interchanged dimer sterically precludes CDK2 binding, providing a possible mechanism regulating CDK2–Cks interactions. One face of the complex exposes the sequence-conserved phosphate-binding region on Cks and the ATP-binding site on CDK2, suggesting that Cks may target CDK2 to other phosphoproteins during the cell cycle.

Introduction

Cell cycle progression is regulated by the activity of cyclin-dependent kinases (Cdks), which consist of ~34 kDa catalytic subunits associated with essential cyclin-regulatory subunits (for recent reviews see Pines and Hunter, 1991; Reed, 1992; Hunter, 1993; Dunphy, 1994; Morgan, 1995). Cdk activity is controlled via regulatory pathways acting through four biochemical mechanisms. Cdk activation involves cyclin binding and the phosphorylation of a conserved threonine (residing between residues 160 and 170 in most Cdk sequences) by the Cdk-activating kinase (CAK) (Solomon et al., 1993; Poon et al., 1993; Fesquet et al., 1993; Fisher and Morgan, 1994; reviewed by Solomon, 1994). Cdk inhibition involves phosphorylation of a conserved threonine–tyrosine pair (Gould and Nurse, 1989) by at least two protein kinases, Wee1 (McGowan and Russell, 1993) and Myt1 (Mueller et al., 1995) and binding of Cdk-inhibitory proteins (reviewed in Hunter and Pines, 1994; Morgan, 1995). The crystal structure of the CDK2–cyclin A complex has recently revealed the mechanism of Cdk activation by cyclin binding. Specifically, cyclin-induced conformational changes in the PSTAIRE helix and the T loop expose the catalytic cleft and CDK2 Thr-160 for CAK phosphorylation (Jeffrey et al., 1995).

Besides both positive and negative regulation by phosphorylation and binding of cyclins and Cdk-inhibitory proteins, Cdks interact with a class of regulatory proteins represented by Cks1 (Cdc28 kinase subunit) in Saccharomyces cerevisiae (Hadwiger et al., 1989) and suc1 (suppressor of cdc2 temperature-sensitive mutations) in Schizosaccharomyces pombe (Hayles et al., 1986a; Hindley et al., 1987). The yeast Cks proteins have essential cell cycle functions, based on genetic analysis. In addition, these proteins are phylogenetically conserved at both the structural and functional levels, as two human homologs, CksHs1 and CksHs2, functionally substitute for Cks1 in S. cerevisiae (Richardson et al., 1990). Although Cks proteins are essential for cell cycle progression in vivo, and have been shown both genetically and in vitro to interact with Cdks (Brizuela et al., 1987; Hadwiger et al., 1989), their precise biological function is an enduring mystery (Morgan, 1995; Endicott and Nurse, 1995). Conflicting activities for Cks homologs have been inferred from different genetic and biochemical experiments. The genetic approaches have included gene disruption (Hayles et al., 1986b; Hindley et al., 1987), overexpression (Hadwiger et al., 1989; Hayles et al., 1986a, 1986b; Moreno et al., 1989), and analysis of temperature-sensitive mutants (Tang and Reed, 1993). Biochemically, suc1 was shown to inhibit Cdk dephosphorylation on Tyr-15 (Dunphy and Newport, 1989). The X-ray structures of three of the Cks proteins (CksHs2 [Parge et al., 1993], suc1 [Endicott et al., 1995; Bourne et al., 1995], and CksHs1 [Arvai et al., 1995a]) have been solved, but they have not revealed the nature of the Cdk-binding interface. However, these structures identify two distinct suc1 conformations: a single domain fold (Endicott et al., 1995) and a β-interchanged dimer (Bourne et al., 1995). Similar dual conformations occur between the CksHs1 single domain fold (Arvai et al., 1995a) and the β-interchanged CksHs2 dimer (Parge et al., 1993).

Here we present the 2.6 Å resolution crystal structure of human CDK2 in complex with the human cell cycle regulatory protein CksHs1. This structure reveals the mode of CDK2 binding to CksHs1, suggests a possible mechanism of cooperativity and self-regulation of Cks proteins during the cell cycle, and implicates Cks as a targeting or match-making protein for Cdks and at least one other phosphoprotein.

Results and Discussion

Structure Determination

The crystal structure of human CDK2 in complex with CksHs1 was determined by molecular replacement in two different crystal forms that yielded identical complexes at low resolution. Monoclinic crystals with space

†Present address: Laboratoire de Cristallographie et de Cristallisation des Macromolécules Biologiques, Centre National de la Recherche Scientifique, Institut de Recherche Concertée 1, 31 Joseph Aiguier, 13402 Marseille Cedex 20, France.

group $P2_1$ ($a = 56.8$ Å, $b = 69.9$ Å, $c = 60.5$ Å, and $\beta = 114.5°$), which contain one CDK2–CksHs1 complex per asymmetric unit, were used to obtain the refined structure, since they gave higher resolution diffraction than the orthorhombic crystals also analyzed. The human CDK2–CksHs1 complex structure was refined at 2.6 Å resolution to a crystallographic R value of 19.8% using all reflections in the 6 Å–2.6 Å resolution range with good stereochemistry (see Experimental Procedures). The excellent quality of the 2.6 Å electron density map unambiguously reveals the positions of the carbonyl oxygens and side chains in CDK2 and CksHs1, as well as at the complex interface (Figure 1A).

Overall Structure of the Complex

The structure of human CDK2 in complex with CksHs1 consists of an N-terminal lobe (N-lobe) (residues 1–85) and a large C-terminal lobe (C-lobe), with the ATP-binding site located in a cleft between the two lobes, as seen for free CDK2 (deBondt et al., 1993). This kinase fold is conserved throughout the entire protein kinase family (Taylor and Radzio-Andzelm, 1994). CksHs1 is folded into four antiparallel β strands (β1 to β4) and two short α helices, with overall dimensions of 35 Å × 25 Å × 35 Å. In sequence order, there is an N-terminal β hairpin followed by an exposed α-helical hairpin, and then a C-terminal β hairpin that results in a four-stranded β sheet, which shows a surprising topological homology with the N-lobe domain of CDK2 (Arvai et al., 1995a).

CksHs1 interacts exclusively with the CDK2 C-lobe and is positioned at the opposite side relative to the structurally homologous CDK2 N-lobe (Figure 1B). This places CksHs1 over 26 Å from CDK2 Tyr-15, suggesting that proposed interference with dephosphorylation of CDC2 Tyr-15 in Cdk–Cks complexes (Hayles et al., 1986a; Dunphy and Newport, 1989; Jessus et al., 1990) is unlikely, but feasible. This CksHs1-binding site is also entirely distinct from the cyclin-binding site located predominantly in the CDK2 N-lobe from the CDK2–cyclin A complex crystal structure (Jeffrey et al., 1995).

The Human CDK2–CksHs1 Interface

CksHs1 binds to the CDK2 C-lobe using all four β strands, the β1–β2 loop, and the β-hinge region to form a continuous saddle-shaped interface across CDK2 helix α5 and loop L14 (Figures 1C, 1D, and 2A). The concave interior face of the CksHs1 four-stranded β sheet envelops the CDK2 helix α5 and the insert loop L14 of 25–30 residues located between helices α5 and α6. Consequently, the CksHs1 β3–β4 loop, defined as the β-hinge region (Bourne et al., 1995), points toward the CDK2 active site cleft, whereas the β1–β2 loop is directed into the solvent at the opposite side of the complex interface (Figure 1C). The Cdk loop L14 is specific to Cdk protein kinases, but, curiously, is also found with weak homology in the mitogen-activated protein kinase, the extracellular signal–regulated kinase 2 (Zhang et al., 1994), and the twitchin kinase (Hu et al., 1994; for review see Goldsmith and Cobb, 1994), whereas L14 is absent in the cAMP-dependent protein kinase (Knighton et al., 1991) and casein kinase I (Xu et al., 1995).

The localization of the CDK2 interface within the sequence-continuous region Asp-206 to Trp-243 suggests that Cks binding is unlikely to trigger any global CDK2 conformational change, which is consistent with the observed similarities of this novel CDK2 structure to existing Cdk structures (Cox et al., 1994; Goldsmith and Cobb, 1994) and with the noninhibitory effect of Cks proteins on Cdk catalytic activity (Moreno et al., 1989; Tang and Reed, 1993). In contrast with the sequence-local CDK2 interface, the Cks interface involves regions throughout the entire sequence, with each β strand contributing interface residues on one surface and phosphate anion–binding site residues (β1 Lys-11, β2 Arg-20, β3 Trp-54, and β4 Arg-71) on the opposite solvent-exposed face (Figures 1C and 1D).

The complex interface extends over 25 Å in a direction roughly parallel to the CksHs1 β3 and involves both hydrophobic and polar interactions. Hydrophobic interactions cluster within the CksHs1 β sheet at the center of the complex interface, with two discrete patches of polar interactions located at each extremity, which result in the formation of 17 hydrogen bonds involving three solvent molecules. The surface area at the complex interface represents a total of 650 $Å^2$ buried to a 1.6 Å radius probe on each protein and is mainly hydrophobic (55%). The complex interface, which buries 14% of the total solvent-accessible CksHs1 surface area, involves 13 CDK2 side chain residues and 17 CksHs1 side chain residues. A cluster of CksHs1 hydrophobic residues (Tyr-12, Tyr-19, Met-23, Tyr-57, Met-58, Ile-66, and Leu-68) plus two histidines (His-21 and His-60) pack closely to CDK2 hydrophobic residues (Ile-209 and Phe-213 in helix α5 and Phe-240, Pro-241, and Trp-243 in loop L14) (Figures 2A and 2B). CDK2 Glu-208 and Ile-209 backbone nitrogens form key charged hydrogen bonds to CksHs1 Glu-63 side chain carboxylate, which also provides remarkable charge complementarity for the positively charged N-cap of CDK2 helix α5 (Figure 2C).

Structural Chemistry for Cdk–Cks Binding Specificity

Compared with the almost identical CksHs1 and CksHs2 homologs (81% identity), the two yeast homologs, suc1 and Cks1, have extensions at both the N- and C-termini and a nine residue insertion in the middle of the protein, resulting in an identity of only 53% (Richardson et al., 1990) (Figure 3A). However, 15 out of the 17 residues responsible for the structural interactions in kinase binding identified here are invariant within the Cks protein family. Thus, the three-dimensional structure of CksHs1

(*Figure 1 legend continued*)

A CksHs1 Cα trace (orange) is shown through the surface and reveals that the buried residues cluster in the interior concave face of the CksHs1 β sheet and in the β1–β2 and β3–β4 loops, which envelop the CDK2 helix α5 and loop L14 (green).

(D) CDK2 molecular surface, with buried residues in helix α5 (green) and loop L14 (cyan); nonburied residues are shown in white. CksHs1 residues involved in the binding interface are shown (orange bonds with red oxygen, blue nitrogen, and yellow sulfur atoms as balls) with a Cα trace (yellow). CksHs1 residues in all four β strands participate in the binding interface.

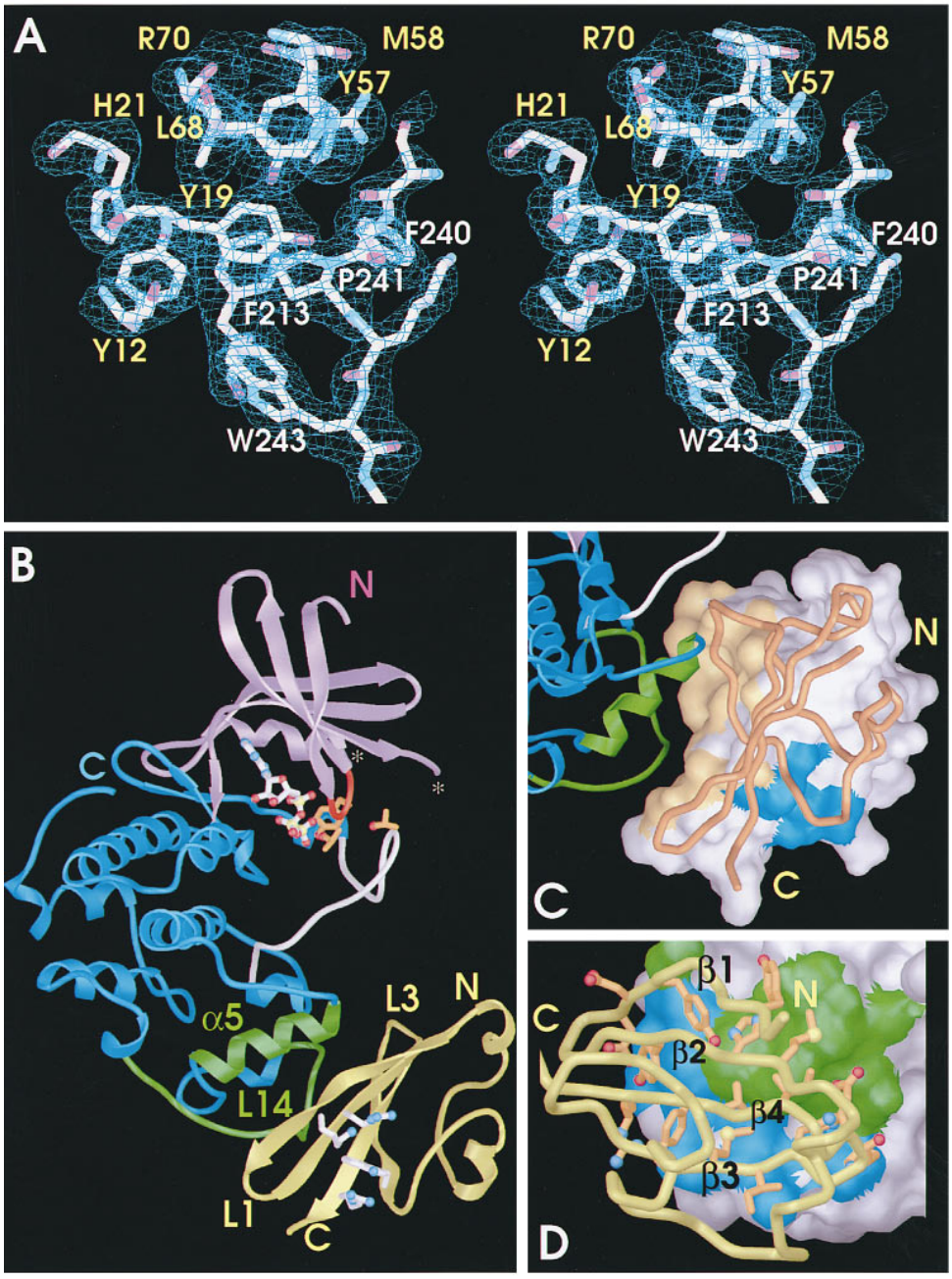

Figure 1. Quality of the Structure and Overall View of the CDK2–CksHs1 Complex

(A) Stereo view of the 2.6 Å resolution omit Fo–Fc electron density map, contoured at 2σ, showing the predominant cluster of hydrophobic residues forming the binding interface. The coordinates of this region (5% of the total number of atoms) were omitted and the protein coordinates were refined by simulated annealing before the phase calculation. Residues are labeled in white for CDK2 and in yellow for CksHs1.

(B) Ribbon diagram of CksHs1 (yellow) bound to CDK2, with the N-lobe in purple and the C-lobe in blue and green. The ATP molecule is displayed at the interface of the two CDK2 lobes (white bonds with red oxygen and blue nitrogen atoms as spheres) and is taken from the free CDK2 coordinates (deBondt et al., 1993). The functional structural elements are color coded for CDK2: the β1–β2 loop, red; the disordered loop to the PSTAIRE sequence in helix α1, asterisks; the T loop, white. Side chains forming the phosphorylation sites in the β1–β2 loop (Thr-14 and Tyr-15) and in the T loop (Thr-160) (orange bonds with red oxygen atoms as balls), as well as the CksHs1 side chains forming the conserved phosphate anion–binding site (β1 Lys-11, β2 Arg-20, β3 Trp-54, and β4 Arg-71) (white bonds with blue nitrogen atoms as balls), are displayed. The CDK2 secondary elements involved in the binding interface are highlighted (green), and CksHs1 loops β1–β2 and β3–β4 are labeled L1 and L3, respectively.

(C) CksHs1 molecular surface, colored with the residues buried to a 1.6 Å probe radius in pale yellow, the nonburied residues in white, and the phosphate anion–binding site in blue. A ribbon diagram of the CDK2 molecule is shown with the color code and orientation as in (B).

(*Figure 1 legend continued on previous page*)

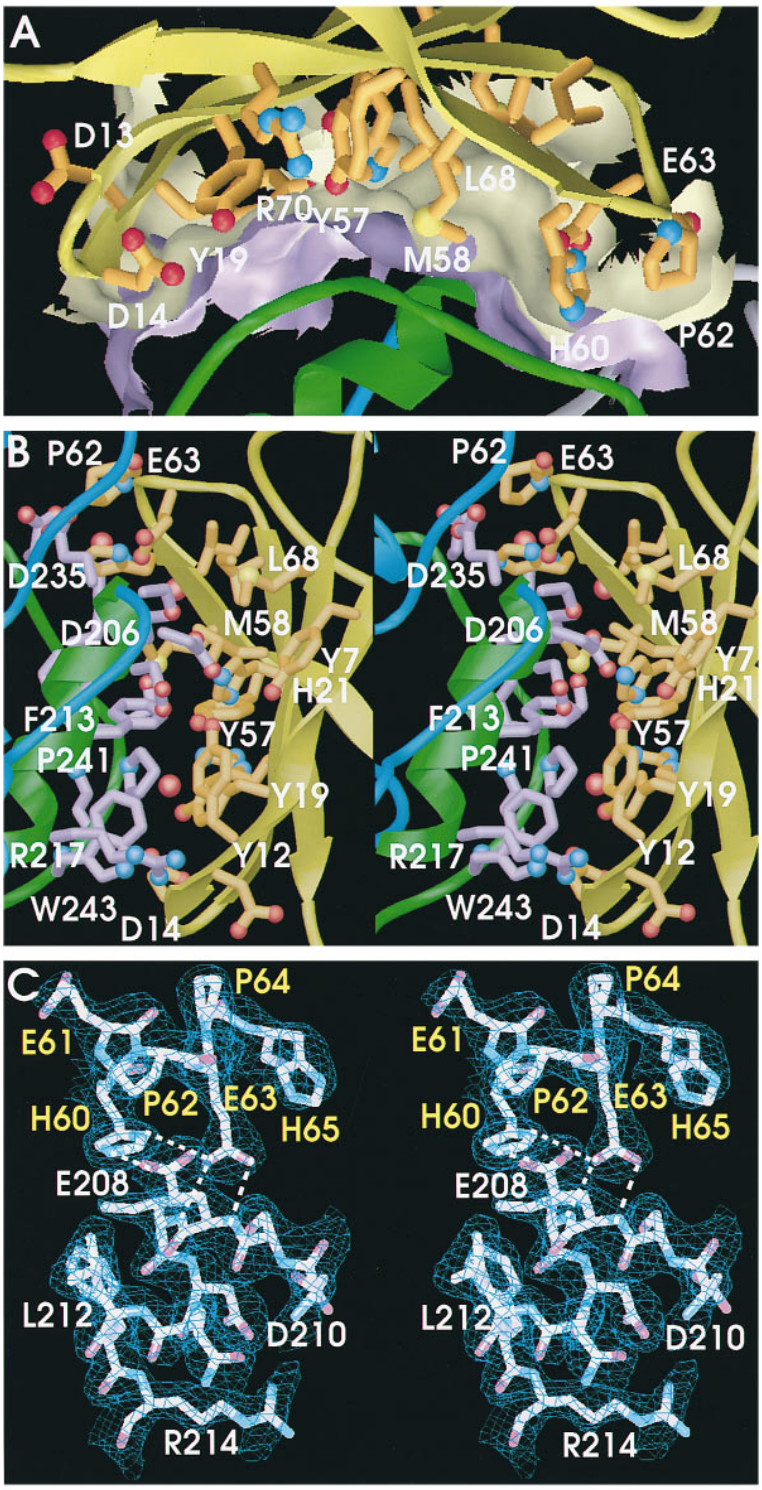

Figure 2. Interface of the CDK2–CksHs1 Complex

(A) Cross-section of the buried molecular surface (purple for CDK2 and pale yellow for CksHs1) at the CDK2–CksHs1 binding interface viewed from CDK2 loop L14, showing the continuous and complementary saddle-shaped interface between CDK2 loop L14 and the interior concave face of the CksHs1 β sheet. Residues that participate in the binding interface are displayed for CksHs1 (orange bonds with red oxygen, blue nitrogen, and yellow sulfur atoms as balls), and molecules are colored as in Figure 1B.

(B) Close-up stereo pair of the CDK2–CksHs1 complex interface, oriented roughly to match Figure 1B and viewed from CDK2 helix α5, with the molecules color coded as in (A). The key complex interface side chains are displayed for CDK2 (purple bonds) and CksHs1 (orange bonds). The alignment of the CksHs1 Glu-63 side chain in the β-hinge region with the direction of CDK2 helix α5 is shown (top). Other polar interactions occur between CDK2 Ser-239 backbone carbonyl and CksHs1 Arg-70 side chain, CDK2 Lys-242 backbone nitrogen and CksHs1 Asp-14 side chain, and CDK2 Trp-243 side chain nitrogen and CksHs1 Asp-13 carbonyl oxygen. An equivalent cluster of polar interactions at the other side of the interface occurs between CDK2 Asp-206 side chain and CksHs1 Tyr-7 hydroxyl and His-21 side chain, CDK2 Glu-208 side chain and CksHs1 His-60 side chain, CDK2 Asp-210 side chain and CksHs1 His-21 side chain, CDK2 Lys-237 side chain and both the CksHs1 Ile-59 backbone carbonyl and the Glu-61 side chain. Three ordered solvent molecules (red spheres) are shown at the binding interface. Two of them (top) establish hydrogen bonds between CDK2 Lys-237 and Asp-235 side chains and CksHs1 Glu-61 backbone nitrogen and side chain atoms and between CDK2 Lys-237 side chain and CksHs1 Tyr-57 carbonyl oxygen and Ile-59 backbone nitrogen atoms. The third one (bottom) is hydrogen-bonded to CDK2 Ser-239 carbonyl oxygen and both CksHs1 Tyr-19 and Arg-70 side chains.

(C) Stereo pair view of the refined σA-weighting 2[Fo–Fc] electron density map (contoured at 1σ) of the CksHs1 β-hinge region in the closed conformation (residues His-60 to His-65) and CDK2 helix α5, oriented to match (A). The CksHs1 His-60 and Glu-63 side chains within the β-hinge region are hydrogen-bonded to residues in the N-cap of CDK2 helix α5 (Glu-208 and Ile-209).

bound to CDK2 is expected to be representative of a biologically important interaction conformation for both human and yeast Cks proteins, and presumably all other Cks proteins. Furthermore, the Cdk residues involved in the complex interface are invariant in both human and yeast kinases (Figure 3B), consistent with earlier evidence that human Cks proteins can functionally replace the single endogenous protein in yeast (Richardson et al., 1990).

The structure of the CDK2–CksHs1 complex suggests the structural basis for Cks binding to the related Cdk protein kinase CDK3 (Meyerson et al., 1992) and the lack of Cks binding to CDK4 or CDK5 (Azzi et al., 1994). Analysis of the amino acid sequences of these three

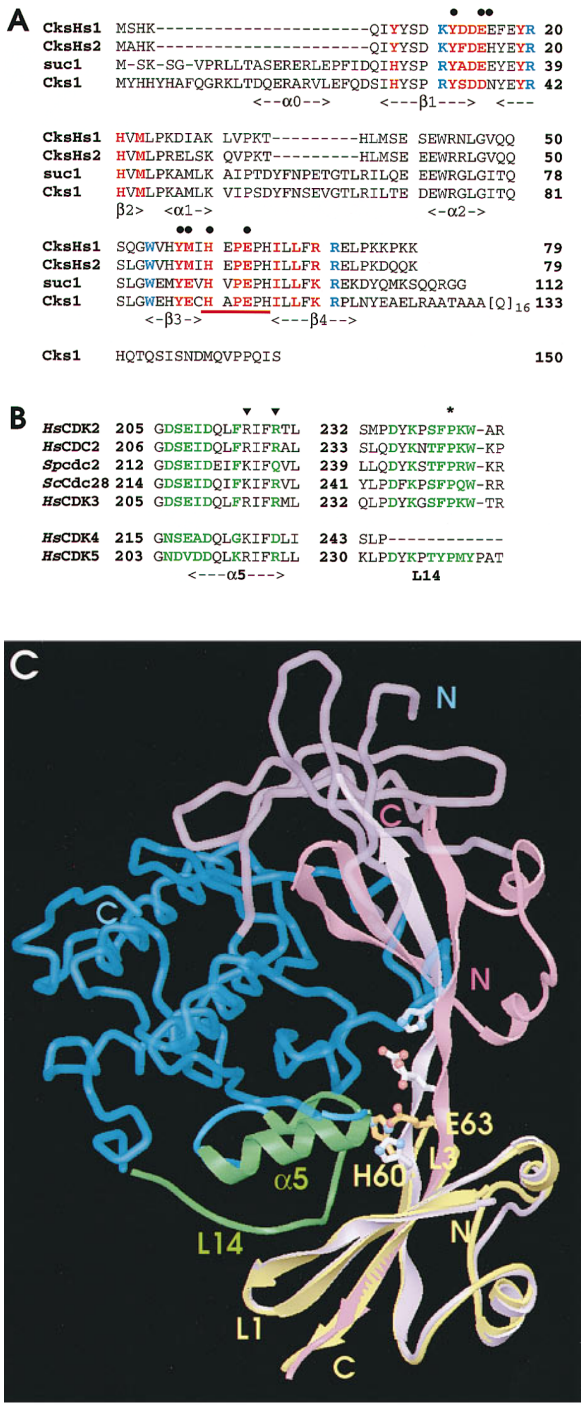

Figure 3. Sequence Conservation and Cks Assembly

(A) The sequences of the two human homologs (CksHs1 and CksHs2) (Richardson et al., 1990) are aligned with those of the two yeast Cks proteins (S. pombe suc1 [Hayles et al., 1986a] and S. cerevisiae Cks1 [Hadwiger et al., 1989]), with the residues involved in the complex formation (red) as well as those involved in the anion-binding site (blue) indicated. The β-hinge region His-60 to His-65 (red bar), which forms a β bend between β3 and β4 in CksHs1, is sequence conserved, but is conformationally different in CksHs2, where it forms an extended conformation promoting a β-strand exchange that interlocks two subunits into a dimer (Parge et al., 1993). The position and identity of the four β strands and helices are indicated beneath the sequence, and residues mutated are identified by closed circles. The only two variations in the Cdk-binding region are found at position CksHs1 Met-58, which is glutamic acid in both suc1 and Cks1, and at position CksHs1 Glu-61, which is valine in suc1 and alanine in Cks1. The Met-58→Glu variation may favor the formation of a hydrogen bond with the cdc2 kinase residue Gln-224 in S. pombe and of a salt bridge with Cdc28 kinase residue Arg-226 in S. cerevisiae without altering complex formation. In contrast, the Glu-61→Val(Ala) variation disrupts the unique salt bridge formed between the CDK2-conserved Lys-237 and the glutamic acid found in human Cks proteins, but likely has little influence on the overall binding interface.

(B) The Cdk sequences are aligned for human CDK2, human CDC2, S. pombe cdc2, S. cerevisiae Cdc28 (deBondt et al., 1993 and references therein), and human CDK3 (Meyerson et al., 1992) in the two regions that form the Cks-binding site (green), as well as for human CDK4 (Khatib et al., 1993) and human CDK5 (Meyerson et al., 1992), which do not bind Cks proteins. Both the nonconservation of the GDSEID and (S,T)FPXW motifs and the lack of the insert region between helices α5 and α6 characterize Cdks that are not regulated by Cks proteins. Suc1-binding sites identified by alanine-scanning mutagenesis of S. pombe cdc2 that match our structure are marked (triangle), as well as the ts mutation Cdc28-1N (Pro-241→Leu) (asterisk).

(C) Ribbon model of the monomeric fold of CksHs1 monomer (yellow) bound to CDK2 (displayed as Cα trace except for helix α5 and loop L14 and oriented to match Figure 1B, with the same color code) with a superimposed CksHs2 interlocked dimer (pink and light purple ribbons). The superimposition, which was done using the Cα atoms of one pair of folding domains (yellow for CksHs1 and light purple for CksHs2), reveals the strikingly different conformation of the β-hinge region. The His-60 and Glu-63 side chains within the β-hinge region are displayed in both Cks assemblies (orange bonds for monomeric CksHs1 and white bonds for β-interchanged dimeric CksHs2) and reveal that the close vicinity of His-60 and Glu-63 side chains, which requires the closed conformation of the β-hinge region, is critical for CDK2 binding. Steric clashes occur between the CDK2 N-lobe (purple Cα trace) and the adjacent subunit in the CksHs2 β-interchanged dimer structure (pink ribbon). Atoms are color coded as in Figure 2A.

protein kinases, which are representative members of three different subfamilies within the Cdk family, revealed a strict conservation of both the GDSEID motif at the beginning of helix α5 and the (S,T)FPXW motif in L14 for CDK3, but not for CDK4 or CDK5 (Figure 3B). In fact, CDK4 lacks the L14 contact region entirely, explaining its lack of Cks binding. These results concerning Cdk subfamily binding to Cks proteins support the importance of the GDSEID and (S,T)FPXW kinase motifs in the binding interface of our CDK2–CksHs1 complex structure.

Possible Structure-Based Self-Regulation of Cks Proteins

The ability of the Cks-conserved β-hinge motif HXPEPH to switch between two distinct conformations may provide a structural mechanism for self-regulation of Cks binding to Cdks. Closing of the β-hinge motif produces the intrasubunit β hairpin and single domain fold, as observed in unbound suc1 (Endicott et al., 1995) and CksHs1 (Arvai et al., 1995a), as well as in this CDK2–CksHs1 complex. Opening the β hinge to its extended conformation may lead to the intersubunit β-strand interchange and the interlocked dimer, as observed in suc1 (Bourne et al., 1995) and CksHs2 (Parge et al.,

1993). This β-hinge conformational switching could regulate Cdk binding, because it markedly alters the Cks interface region in terms of its key residue accessibility, steric compatibility, and side chain arrangements.

The CksHs1 single domain fold resulting from the closed β-hinge conformation exposes at the β sheet surface several conserved hydrophobic side chains (Tyr-12, Tyr-17, Tyr-57, Met-58, Ile-66, and Leu-68) that are crucial for the kinase interaction defined by our structure. In contrast, the hexameric CksHs2 structure, resulting from the open β-hinge conformation, sequesters these side chains within an internal channel (Parge et al., 1993), preventing any access for kinase binding. Similarly, the two suc1 crystal structures reveal that the single domain fold exposes the same conserved hydrophobic residue cluster at the molecular surface as in CksHs1 (Endicott et al., 1995), and the β-interchanged dimeric fold sequesters this cluster within a cavity, as in CksHs2 (Bourne et al., 1995).

Superimposition of the β-interchanged suc1 or CksHs2 dimers with the single domain fold of CksHs1 bound to CDK2 reveals several steric clashes between the CDK2 N-lobe and the adjacent subunit in the Cks dimer, suggesting that the Cks β-interchanged dimer fold cannot bind CDK2 (Figure 3C). Moreover, the critical role played by CksHs1 His-60 and Glu-63 side chains in the binding interface, located in the β-hinge region, is apparently blocked by their different arrangement in the extended conformation of the β-hinge HXPEPH motif found in the β-interchanged Cks structures (Figure 3C). These observations are supported by gel filtration chromatography experiments on both the monomeric and dimeric forms of suc1 in the presence of CDK2, which show no CDK2–suc1 complex formation with the β-interchanged dimeric form of suc1 (data not shown), and by similar results with BIAcore affinity measurements (M. H. W. and S. I. R., unpublished data). Thus, the CDK2–CksHs1 complex structure reveals a potential structural mechanism for self-regulation of Cks binding, which could be triggered by alterations in the chemical environment of the cell associated with cell cycle transitions (provided the β-interchanged dimer exists in vivo).

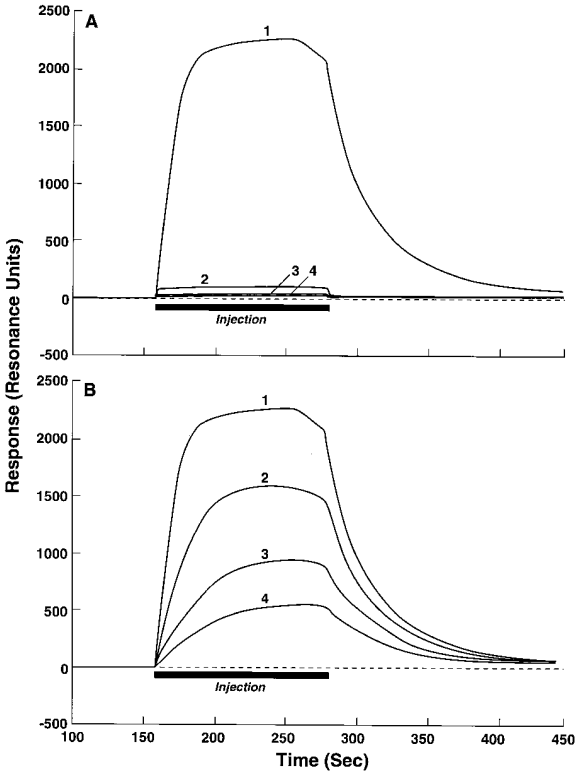

Figure 4. Binding Affinity Measurements

BIAcore binding data for the interaction of CDK2 with wild-type CksHs1 and mutants.

(A) The resonance signal is plotted as a function of time for the injection of 200 nM CDK2 over a sensor chip coupled with CksHs1 (1), CksHs1 Glu-63→Gln (2), CksHs1 Tyr-57→Ser, Met-58→Ala, His-60→Asp, and Glu-63→Lys (3), and CksHs1 Tyr-12→Lys, Asp-14→Lys, and Glu-15→Lys (4).

(B) The resonance signal is plotted as a function of time for the injection of CDK2 at concentrations of 200 nM (1), 100 nM (2), 50 nM (3), and 25 nM (4) over a sensor chip coupled with CksHs1. The injection period is indicated by a solid bar.

Mutational Analysis of the CDK2–CksHs1 Interface

The structure of the CDK2–CksHs1 complex suggests biochemically and biologically important contact residues. A temperature-sensitive (ts) mutation in the S. cerevisiae Cdk gene *CDC28*, *cdc28-1N*, substitutes the loop L14 Pro-250 to leucine (CDK2 residue 241). Based on our CDK2–CksHs1 complex structure, this mutation likely disrupts the tight cluster of aromatic residues located in the central region of the binding interface (CDK2 Phe-213, Pro-241, and Trp-243 and CksHs1 Tyr-12, Tyr-19, and Tyr-57), rather than interfering with cyclin binding, as earlier proposed (Surana et al., 1991). The phenotype conferred by this mutation is atypical for ts *cdc28* mutations, as cells arrest predominantly in G2 rather than in G1. *cks1* ts mutations confer a remarkably similar phenotype, both in terms of cell cycle arrest (predominantly in G2) and cell morphology. Interestingly, ts Cks1 mutant proteins contain substitutions at positions important for Cdk binding (e.g., *cks1* ts-3 [Met-46→Arg], *cks1* ts-7 [Arg-104→Gln], *cks1* ts-35 [Asp-37→Gly], *cks1* ts-38 [Ser-36→Asp, Asn-39→Tyr], and *cks1* ts-42 (Met-46→Thr]) (Figure 3A; Tang and Reed, 1993). These observations suggest that Cdc28-1N is specifically defective in Cks1 interaction, accounting for its biological defect, and that, conversely, Cks1 mutants ts-3, ts-7, ts-35, ts-38, and ts-42 might be defective in Cdk interaction. Consistent with the interpretation based on our structure, the Cdc28 kinase isolated from the *cdc28-1N* mutant is not temperature sensitive in vitro (Surana et al., 1991), arguing against a defect in cyclin binding. Likewise, Cdc28 kinase isolated from *cks1* ts mutants is not temperature sensitive, suggesting that interaction between the two proteins involving CDK2 Pro-241 (Cdc28 Pro-250) is essential for cell cycle progression, but not for an active kinase.

To test further the biological importance of the structure-based model, we constructed three mutant alleles of CksHs1 intended to decrease interactions with CDK2. In the first, a single site charge change (Glu-63→Gln) removes the favorable glutamic acid carboxylate interactions with CDK2 Glu-208 and Ile-209 backbone nitrogens. A second mutant with more extensive changes

Table 1. CDK2–CksHs1 Estimated Equilibrium Dissociation Constant and Rate Constants

CksHs1 Ligand	K_d (M)	k_{on} ($M^{-1}s^{-1}$)	k_{off} (s^{-1})
Wild type	7.7×10^{-8}	3.2×10^{5}	2.5×10^{-2}
Tyr-12→Lys, Asp-14→Lys, Glu-15→ Lys	UD	UD	UD
Glu-63→Gln	UD	UD	UD
Tyr-57→Ser, Met-58→Ala, His-60→Asp, Glu-63→Lys	UD	UD	UD

The numbers presented are mean values, and the uncertainties from the fitting procedures were less than 10% of the values. UD indicates that the level of CDK2 binding was below that required for calculation of rate constants. All kinetics experiments were done in triplicate.

had four interface substitutions, Tyr-57→Ser, Met-58→Ala, His-60→Asp, and Glu-63→Lys. In the third, Cks residues Tyr-12, Asp-14, and Glu-15 were modified to lysine to disrupt both hydrophobic and polar interactions of CksHs1 with CDK2. The affinities of wild-type and mutant CksHs1 for CDK2 were measured in two ways. First, a dissociation constant (K_d) was determined using the BIAcore surface plasmon resonance detection system. The K_d for wild-type CksHs1 was determined by titrating CDK2 against a fixed amount of immobilized CksHs1 and measuring the interaction (Figure 4). The K_d for wild-type CksHs1 was 7.7×10^{-8} M, consistent with isothermal calorimeter experiments (data not shown), whereas for Glu-63→Gln, the level of binding detected (Figure 4A) was too low to calculate a K_d. For both of the multiple mutations (Tyr-12→Lys, Asp-14→Lys, and Glu-15→Lys and Tyr-57→Ser, Met-58→Ala, His-60→Asp, and Glu-63→Lys) no binding was detectable (Table 1). Thus, all of the mutant proteins were defective in binding CDK2 in vitro. Next, we measured the in vivo binding of mutant and wild-type CksHs1 to the endogenous Cdk of budding yeast, Cdc28, which has all Cks contact residues conserved, using the yeast two-hybrid system (Table 2). All three mutant alleles were, again, strongly defective in interacting with Cdc28, as predicted. Conversely, we used the two-hybrid system to measure the affinity of ts mutant Cdc28-1N (Pro-250→Leu) for Cks1. Compared with wild-type Cdc28, Cdc28-1N indeed showed severely reduced binding to Cks1 (Table 2). The similar expression of all of these two-hybrid fusion proteins was confirmed by Western blotting, supporting the relevance of the observed reduced binding. Finally, we tested the biological consequences of the three Cdk binding–defective mutant alleles of *CksHs1* and found them incapable of replacing the endogenous gene in yeast (Table 2). Because the Glu-63→Gln-substituted structure of the homologous human protein CksHs2 is identical to wild type, Glu-63 mutations apparently do not cause the nonfunctional biological phenotype by structural alterations (M. H. W., Y. B., A. S. Arvai, J. A. T., and S. I. R., unpublished data). Taken together, these results suggest that binding to Cdks is a critical function of Cks proteins and that the CDK2–CksHs1 interface identified here represents a biologically important interaction.

Previously, experiments on S. pombe cdc2 kinase have attempted to locate the suc1-binding site by extensive alanine-scanning mutagenesis (Ducommun et al., 1991; Marcote et al., 1993). These studies suggested that the suc1-binding site involved both the N- and C-lobes of cdc2, although removal of the L14 insert between cdc2 helices α5 and α6 dramatically altered suc1 binding (Ducommun et al., 1991). Our structure shows that most of the sites implicated by cdc2 mutagenesis do not lie in the interface and therefore, when mutated, probably affect Cks binding indirectly. Only the Arg-214→Ala and Arg-217→Ala mutations in the CDK2 C-lobe, which eliminate suc1 binding without altering the kinase activity, are consistent with the interface region revealed by the CDK2–CksHs1 complex structure. The CDK2 Arg-217 stacks against the side chains of CDK2 Trp-243 and CksHs1 Tyr-12, two key residues at the complex interface. The Arg-214 side chain is not directly involved in CksHs1 binding, but it stabilizes the conformation of the two aspartate residues, Asp-206 and Asp-210, within the GDSEID motif. Thus, most of the contact sites implicated by the alanine-scanning mutagenesis results may reflect complex, indirect effects within the two-domain kinase structure.

Exposed Sequence-Conserved Residues Not Involved in Cdk Binding

Besides the cluster of exposed conserved hydrophobic residues forming the contact with Cdk, the Cks proteins have a conserved and highly positive pocket of residues (CksHs1 Lys-11, Arg-20, Trp-54, and Arg-71) that forms

Table 2. β-Galactosidase Activities of CDC28/Cks in the Two-Hybrid Assay and In Vivo Rescue of *cks1* Disruption by CksHs1 Mutants

Activation Domain Fusion	DNA-Binding Domain Fusion (%)[a]		Rescue of *cks1* Disruption[b]
	Cdc28	Cdc28-1N	
Cks1			
Wild type	100	4.5 ± 1.8	
CksHs1			
Wild type	100		+
Tyr-12→Lys, Asp-14→Lys, Glu-15→Lys	9.2 ± 1.1		−
Glu-63→Gln	16.2 ± 4.3		−
Tyr-57→Ser, Met-58→Ala, His-60→Asp, Glu-63→Lys	3.7 ± 0.9		−

[a] The β-galactosidase activities represent the mean and standard deviation of four independent experiments each and are expressed as a percentage of the activity of the wild-type protein.
[b] The CksHs1 proteins were assayed for their ability to rescue the *cks1* disruption as described in Experimental Procedures.

a phosphate anion–binding site exposed on the other side of the molecule relative to the complex interface, based upon structures of phosphate and the phosphate analog vanadate bound to CksHs1 (Arvai et al., 1995a). This result does not support the hypothesis of Cks binding to the CDK2 Thr-160 phosphate group or of Cks oligomerization of Cdks (Parge et al., 1993). Thus, the interlocked dimeric (or hexameric) form of Cks proteins may represent a negative regulation of Cdk–Cks interaction or a distinct non-Cdk-related function for Cks proteins. Such a hypothesis of two distinct functions for the Cks proteins has been independently proposed (Jessus et al., 1990). Our CDK2–CksHs1 structure positions the Cks phosphate anion–binding site on the same side of the Cdk catalytic site, in a cleft between the two lobes, thus forming an extended recognition surface flanking the CDK2 catalytic site (Figures 1B and 5). Also, exposed in the groove adjacent to the phosphate anion–binding site, conserved Cks residues (Ile-6, Tyr-8, Glu-18, Pro-25, Gln-50, and Ser-51) expand the conserved, exposed surface that could participate in Cks binding to a second protein. This suggests that Cks proteins act in targeting Cdks to substrates or other phosphorylated proteins.

The CDK2–Cyclin A–CksHs1 Ternary Complex

Superimposition of CDK2 bound to CksHs1 with the CDK2–cyclin A complex (Jeffrey et al., 1995) generates a model for the ternary Cdk macromolecular assembly (Figure 5). This model shows that the two binding sites are distinct from each other and suggests that a ternary complex can form within the cell, a result observed in solution (data not shown). The model reveals a bowl-shaped groove 20 Å in diameter, limited on each side by the cyclin A and CksHs1 molecules, and positions the CDK2 Thr-160 residue at the bottom center of the groove. This groove is bordered by three lysine residues of CksHs1 (Lys-26, Lys-30, and Lys-34) and two of cyclin A (Lys-226 and Lys-417), all pointing toward the CDK2 active site cleft (Figure 5A). In addition, CksHs1 Pro-62 is located only 7.5 Å away from CDK2 Thr-160 and faces the cyclin A loop 269–272, also ~8 Å away from CDK2 Thr-160. Thus, Cks binding could possibly restrict access of CAK, the Cdk that phosphorylates Thr-160, which is likely to have dimensions similar to CDK2 (about 65 Å × 45 Å × 25 Å); thus, within the cell there may be an obligatory order of events in which Cdk phosphorylation precedes Cks binding. Similarly, Cks binding could potentially interfere with the Cdk-associated phosphatase KAP, which dephosphorylates CDK2 Thr-160 when cyclin is degraded (Poon and Hunter, 1995).

Structural Changes in CDK2 and CksHs1 upon Binding

Free CDK2 resembles that bound to CksHs1 except for small domain movements (root-mean-square deviation [rmsd] of 0.9 Å for 279 Cα atoms and 0.59 Å for 204 Cα atoms of the CDK2 C-lobe). The largest differences (up

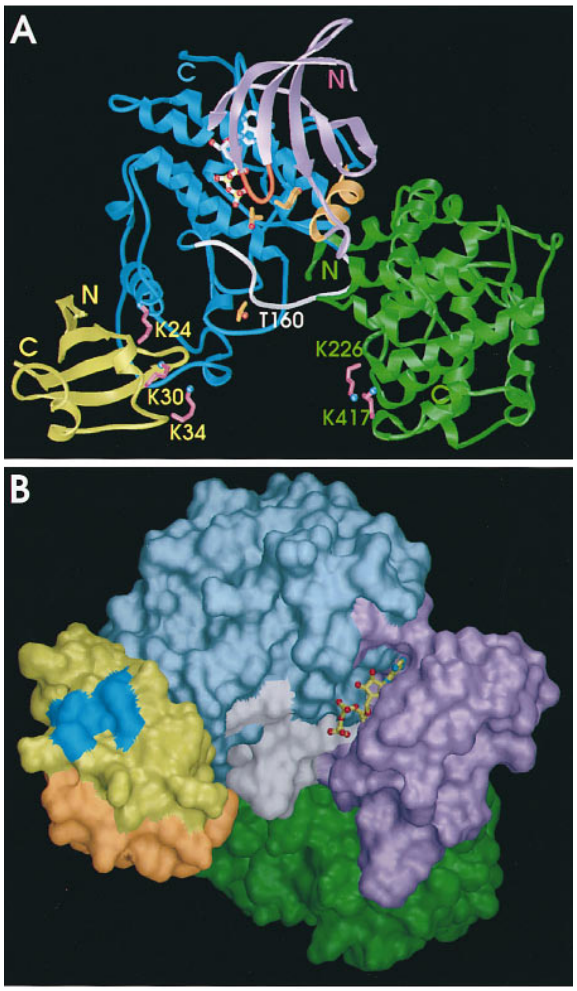

Figure 5. The CDK2–Cyclin A–CksHs1 Ternary Complex

(A) Ribbon diagram of a CDK2–cyclin A–CksHs1 complex model based on the coordinates of our CDK2–CksHs1 complex and those of a CDK2–cyclin A complex (Jeffrey et al., 1995) in which the two CDK2 molecules were superimposed based on the Cα atoms of the C-lobe. Besides two distinct binding sites for cyclin A and CksHs1 at the molecular surface of CDK2, this model reveals a large bowl-shaped groove centered around the phosphorylation site at Thr-160 (middle) in the activated conformation of the CDK2 T loop and bordered by cyclin A and CksHs1 molecules. The presence of positively charged residues (Lys-24, Lys-30, and Lys-34 in CksHs1 and Lys-226 and Lys-417 in cyclin A) located on each side of the groove is displayed (purple bonds and blue for nitrogen atoms as balls). The molecules and the functionally important elements in CDK2 are color coded as in Figure 1B, with cyclin A in green. ATP is taken from the CDK2–cyclin A complex coordinates previously described (Jeffrey et al., 1995).

(B) Molecular surface of the CDK2–cyclin A–CksHs1 complex oriented ~90° away from that in (A), with the same color code. The CksHs1 phosphate anion–binding site (blue) is exposed into the solvent and located on the same side of the CDK2 catalytic site with the ATP molecule bound between the two lobes, thus forming a continuous surface for recognition of a Cdk substrate or other phosphoproteins. The two CksHs1 α helices (orange) are also solvent accessible. The T loop (white), containing the phosphorylation site at position Thr-160 (middle), protrudes at the interface of CksHs1 and cyclin A. Figures 1B–1D, 2A and 2B, 3C, and 4 were generated with the Application Visualization System (AVS) (Advanced Visual Systems, Waltham, Massachusetts), and Figures 1A and 2C were generated with TURBO-FRODO (Roussel and Cambil-

lau, 1989). The solvent-accessible surfaces were calculated with MS (Connolly, 1983), and the ribbon diagrams were generated using RIBBONS (Carson, 1991) implemented in AVS.

to 3 Å) occur in the N-termini (residues 1–9) and in the loops connecting the N-lobe β strands, but they apparently reflect the domain flexibility previously seen for the protein kinase family (Goldsmith and Cobb, 1994) rather than the effect of Cks binding. Our structure also shows an N-lobe conformational change of CDK2 residues 36–39 compared with free CDK2, which adopt a conformation similar to that of the activated CDK2 bound to cyclin A (Jeffrey et al., 1995). In our CDK2–CksHs1 complex structure, the Leu-37 side chain points toward a hydrophobic cluster (Ile-37, Ile-49, Leu-76, and Phe-152), whereas Leu-37 points in an opposite direction in free CDK2. However, the remaining residues preceding the PSTAIRE sequence in the N-lobe and the T loop residues in the C-lobe are disordered in our crystal structure in the absence of cyclin (Figure 1B), as in the free CDK2 structure (deBondt et al., 1993). Similarly, no major changes are seen in the bound Cks conformation. Thus, any allosteric effects on either CDK2 or Cks from CDK2 binding would be subtle, if they occurred at all.

Although CksHs1 binding to CDK2 does not induce dramatic conformational changes, some local changes occur at the binding interface. A rigid-body motion is observed for CDK2 residues 219–251, located in L14 and helix α5. The largest deviations (up to 2 Å) occur at position Ser-239 and appear to be related to CDK2 rearrangements upon CksHs1 binding. Similarly, the most significant CksHs1 change occurs at the tip of loop β3–β4, which shifts by 2.5 Å–3 Å within the CDK2 binding site (an rmsd of 0.85 Å for 69 Cα atoms).

Significance and Implications

The 2.6 Å resolution structure of the CDK2–CksHs1 complex defines the interface region as confined to the Cdk sequence–adjacent C-lobe helix α5 and loop L14. This interface, confirmed by mutagenesis as critical for biochemical and biological Cks–Cdk interactions, is consistent with the observation that Cks association with Cdks is not known to block the binding of any other protein to Cdks. Structural changes are localized to the interface region on both molecules, indicating that Cks proteins are not likely to function in Cdk regulation by inducing a conformational change in the kinase. Rather, Cks proteins present one conserved region to the Cdk interface, leaving the second sequence-conserved region exposed and continuous with the CDK2 active site face. Cks binding, therefore, provides a sequence-conserved phosphate-binding region that forms an expanded recognition surface for the CDK2 catalytic site.

Our structure thus implicates Cks as acting in targeting the Cdk to other proteins or macromolecular assemblies. However, the relatively moderate affinity of CksHs1 for inactive Cdk2 as determined by biophysical methods ($K_d = 7.7 \times 10^{-8}$ M) allows for the possibility that complexes with activated Cdks could be more favored in vivo. This, coupled with the observation that CAK would be sterically prevented from phosphorylating Thr-160 on Cks-bound CDK2, leads to a hypothesis for complex formation and Cdk function. First, cyclin association would promote phosphorylation of the Cdk by CAK (Jeffrey et al., 1995). Cyclin binding and phosphorylation of Cdk might place the T loop in contact with Cks, thereby enhancing the interaction. Second, the higher affinity of Cks proteins for active kinase might restrict the proposed targeting function of Cks proteins to kinase molecules capable of phosphorylating substrates. Such targeting functions may direct the active kinase to substrates or other regulatory proteins. With the nature of the Cks–Cdk interaction defined, the role of Cks in such Cdk substrate recognition and targeting processes and in cell cycle progression can be tested by combined genetic and biochemical studies.

Experimental Procedures

Site-Directed Mutagenesis

Specific amino acid changes were introduced into the human *CKSHS1* gene, contained in the bacterial expression plasmid pRK171 (Rosenberg et al., 1987), using the Transformer mutagenesis kit (Clontech Laboratories) as described by the manufacturer. The mutagenic primers were as follows: Y12KD14KE15K, 5′-cgatact caaactccttttttgtctttttttgtccgaatag-3′; Y57SM58AH60DE63K, 5′-gcaa gatgtgaggttttggttcatcgatcgcagaatggacccatccc-3′; E63Q, 5′-gcaag atgtgaggttgtggttcatgg-3′. The mutant *CKSHS1* sequences were amplified by PCR using flanking oligonucleotides containing BamHI restriction sites, and the products were cloned into the yeast galactose-inducible plasmid YCpG2 (Richardson et al., 1990) and the two-hybrid *GAL4* transcriptional activation domain plasmid pACT2. The resulting constructs were confirmed by DNA sequencing, and mutant CksHs1 proteins were purified as previously described for the wild-type protein (Arvai et al., 1995b).

Two-Hybrid Assays

CKSHS1 wild-type and mutants and S. cerevisiae *CKS1* were cloned into the BamHI restriction site in the polylinker of the plasmid pACT2 to yield *GAL4* transcriptional activation domain fusion constructs tagged with the hemagglutinin (HA) epitope and carrying the *LEU2* gene. S. cerevisiae *CDC28* and *cdc28-1N* open reading frames were cloned into the BamHI restriction site in the polylinker of the plasmid pAS1 (Durfee et al., 1993) to produce a *GAL4* DNA-binding domain fusion construct tagged with the HA epitope and carrying the *TRP1* gene. The pACT2 constructs were transformed into the haploid S. cerevisiae strain Y190 (*MATa gal4 gal80 his3 trp1-901 ade2-101 ura3-52 leu2-3,112+ URA3::GAL→lacZ, LYS2::GAL(UAS)→HIS3-cyh*^{r}) and selected on plates lacking leucine. The pAS1 constructs were transformed into the haploid strain Y187 (*MATα gal4 gal80 his3 trp1-901 ade2-101 ura3-52 leu2-3,112 met*$^-$*URA3::GAL→lacZ*) and selected on plates lacking tryptophan. Yeast transformations were performed as described by Elble (1992). The expression of the fusion proteins was confirmed by Western blotting using a monoclonal antibody (12CA5) to the HA epitope.

Yeast cells (haploid or diploid) containing both pAS1-CDC28 and pACT2-CKSHS1 are not viable, making it impossible to maintain strains containing both plasmids (M. H. W. and S. I. R., unpublished data). Therefore, the method of "quantitative mating" was used to measure the interaction between the fusion proteins in newly formed zygotes produced from mating haploid cells containing the individual plasmids. Y187 cells (5×10^7) containing the pAS1-CDC28 construct were vacuum filtered onto 0.45 mm Metricel membranes (Gelman Sciences). Y190 cells (5×10^7) carrying the pACT2-CKSHS1 constructs were filtered over the layer of Y187 cells, and the filter was then placed onto a YEPD plate containing 1 M sorbitol with the cell side up and incubated at 30°C. After 5 hr, the filter was placed into a 50 ml conical tube with 10 ml of YEPD media and vortexed to resuspend the cells. The filter was discarded, and a sample of the cells was fixed in formaldehyde for microscopic scoring of the percentage of zygotes. The mating efficiency typically ranged between 10% and 20%. The same procedure was performed to measure the interaction between pAS1-CDC28 or pAS1-cdc28-1N with pACT2-CKS1. The cells were pelleted by a 10 min spin at 1000 rpm in a clinical centrifuge. Extracts were prepared by resuspending the pellets in 150 μl of 100 mM Tris–HCl (pH 8), 20% glycerol (v/v), 1 mM β-mercaptoethanol, 1 μg/ml leupeptin, 1 mM PMSF, 1 μg/ml

pepstatin A, and 2 μg/ml aprotinin. Glass beads (0.5 mm diameter) were added to the level of the meniscus and vortexed five times for 30 s, with 30 s intermissions on ice. Extracts were clarified by a 15 min spin at 14,000 × g and then frozen in liquid nitrogen and stored at −70°C. Protein concentrations were measured using the Bradford assay (Bradford, 1976). β-Galactosidase activity was measured using a chemiluminescent assay with the Galacto-Light Plus system (Tropix) following the procedure suggested by the manufacturer. In brief, 5–20 μl of extract was added to 100 μl of diluted Galacton and incubated at room temperature for 30 min. We added 100 μl of accelerator solution and measured chemiluminescence in duplicate for 5 s using a Lumat LB9501 luminometer. The chemiluminescent signal was normalized for the amount of protein and the percentage of zygotes and expressed as a percentage of β-galactosidase activity relative to wild-type CksHs1. We performed three to five independent matings for each experiment.

In Vivo Rescue of *cks1* Disruption

The ability of the mutant *ckshs1* alleles to function in vivo was tested in a yeast strain that has the chromosomal *cks1* gene disrupted and is kept alive with a plasmid containing a wild-type copy of *CKS1*, *cks1::LEU2* (*CEN TRP1 CKS1*) (Richardson et al., 1990). Haploid cells were transformed with the inducible vector YCpG2 containing the specific *ckshs1* mutant under the control of the *GAL1* promoter and carrying the *URA3* gene. Transformants were selected based on tryptophan and uracil prototrophy and were switched to growth for several generations on medium containing galactose (to allow expression of the mutant *ckshs1* alleles from the *GAL1* promoter) and tryptophan (to allow loss of the wild-type *CKS1* gene and the *TRP1* marker). Loss of the plasmid containing the wild-type *CKS1* gene was monitored by plating and testing colonies for tryptophan auxotrophy.

Binding Affinity Measurements

Experiments were performed using surface plasmon resonance technology on a BioSensor BIAcore instrument (Pharmacia). Purified CksHs1 wild-type and mutant proteins were coupled through primary amine groups to the activated carboxyl groups of CM5 sensor chips according to the procedures of the manufacturer. The matrix surface was activated with a mixture of 50 mM N-hydroxysuccinimide (NHS) and 200 mM N-ethyl-N′-(3-diethylaminopropyl)-carbodiimide (EDC) for 7 min at a flow rate of 5 μl/min. Wild-type or mutant CksHs1 at a concentration of 0.1 mg/ml in 10 mM N-2-hydroxyethylpiperazine-N′-2-ethanesulfonic acid (HEPES) (pH 7.4) and 3.4 mM ethylenediaminetetraacetic (EDTA) was injected over the matrix for 7 min at 5 μl/min. Deactivation of the matrix was achieved with 1 M ethanolamine hydrochloride (pH 8.5) for 7 min at 5 μl/min. The immobilization yield of the protein was monitored from the increase in resonance units during the coupling procedure. After each binding experiment, the surface of the sensor chip was regenerated by washing with 50% ethylene glycol, 0.5 M NaCl (pH 7.4) (Kusubata et al., 1992). Binding sensorgrams for the interaction of CksHs1 wild-type and mutant proteins were created using concentrations of CDK2 ranging from 5 nM to 5 μM in 10 mM HEPES pH (7.4), 3.4 mM EDTA, 150 mM NaCl, and 0.001% surfactant P-20. The sensorgrams were analyzed using the BIAevaluation software. Association (k_{on}) and dissociation (k_{off}) rate constants were calculated using the association and dissociation phases of the sensorgrams, respectively. The K_d values were calculated using the equation $K_d = k_{off}/k_{on}$. All kinetic experiments were done in triplicate.

Protein Purification, Crystallization, and X-Ray Diffraction Data Collection

Human CDK2 was expressed in insect cells (T.ni cells) using a baculovirus vector. The cells were lysed and centrifuged, and the clarified supernatant was directly loaded onto an HS column (Poros) equilibrated with buffer A (25 mM HEPES [pH 7.4], 25 mM NaCl, 1 mM EDTA) and a cocktail of protease inhibitors. CDK2 was eluted with 100 mM NaCl in the same buffer and concentrated before loading onto a S-75 Superdex column equilibrated with buffer B (20 mM HEPES [pH 7.4], 200 mM NaCl, 1 mM dithiothreitol [DTT]). The same batch of CksHs1 protein, which was prepared for the crystallization of free CksHs1, was used in this study (Arvai et al., 1995b). The complex was prepared by mixing CDK2 and CksHs1 in a 1:2 ratio, followed by incubation for 30 min at 4°C and then by gel filtration chromatography on a Sephacryl S100 column (Pharmacia) equilibrated with 10 mM HEPES (pH 7.4), 150 mM NaCl, 5% glycerol, 1 mM EDTA, and 1 mM DTT. The CDK2–CksHs1 fractions, which were found at an apparent molecular mass of 44 kDa (corresponding to a 1:1 complex, consistent with cross-linking experiments between cdc2 and suc1 [Ducommun et al., 1991]), were analyzed by 12% SDS–polyacrylamide gel electrophoresis, concentrated to 15–20 mg/ml under nitrogen using an Amicon concentrator with a 10 kDa membrane cutoff, and stored at −70°C.

Crystals were obtained by the vapor diffusion technique at 20°C after mixing an equal volume of the complex with the well solution containing 17%–19% polyethylene glycol monomethyl ester (MEPEG) 5K, 100 mM Tris (pH 7.5), and 100 mM KCl. Crystals grew within 1 day, and two different crystal forms, here termed A and B, were frequently observed in the same drop. Form A crystals belong to the orthorhombic space group $P2_12_12_1$ with cell dimensions a = 62.2 Å, b = 70.1 Å, and c = 102.4 Å and contain one CDK2–CksHs1 complex in the asymmetric unit. A 2.8 Å resolution diffraction data set, which consisted of 93,477 observations for 10,699 unique reflections (93% complete, R_{sym} = 8.9%), was collected on form A crystals using a Fuji plate detector at the 1-5 beamline of the Stanford Synchrotron Radiation Laboratory. Form B crystals belong to the monoclinic space group $P2_1$ with cell dimensions a = 56.8 Å, b = 69.9 Å, c = 60.5 Å, and β = 114.5° and also contain one CDK2–CksHs1 complex in the asymmetric unit. A 2.6 Å resolution data set, which consisted of 84,909 observations for 13,023 unique reflections (97% complete, R_{sym} = 10%), was collected on form B crystals using a Mar-Research imaging plate detector mounted on a Siemens rotating anode operating at 50 kV × 100 mA. Both diffraction data sets were collected at −170°C, and the crystals were previously transferred to 18% MEPEK 5K, 15% ethylene glycol, and 100 mM Tris (pH 7.5) before being flash cooled. Data sets were processed with the programs DENZO and SCALEPACK (Otwinowski, 1993).

Structure Determination and Refinement

Initial phases for the form A data set were obtained by the molecular replacement method using the human CDK2 model (deBondt et al., 1993) and the CksHs1 model (Arvai et al., 1995a) as search models with the AMoRe program package (Navaza, 1994). Phases from the positioned CDK2 molecule (correlation = 37%, R factor = 46% in the 15 Å–3.5 Å resolution range) allowed the positioning of CksHs1 within the cell, giving a final correlation and an R factor of 43% for the two molecules. However, refinement of this model with the X-PLOR program (Brünger et al., 1987) resulted in both high R factor (25%–27%) and R-free (43%–45%) values, associated with poorly defined electron density maps. The space group was then reexamined, based on the presence of a 2-fold axis along the a axis, but refinement in the space group $P2_12_12$ (a = 70.1 Å, b = 102.4 Å, and c = 62.2 Å) resulted in the same problem, and thus suggested the presence of twin crystals.

The structure of form B was determined by the molecular replacement method with the AMoRe program, using either the solution from model A or the original coordinates. In both cases, a clear solution was detected with a correlation of 54% and an R factor of 40% in the 15 Å–3.5 Å resolution range. This model was first refined by rigid-body motion with the CDK2 N-lobe (residues 1–80), the CDK2 C-lobe (residues 87–296), and the entire CksHs1 (residues 5–72) as separate groups, followed by simulated annealing using X-PLOR and manual fitting into σA-weighting electron density maps (Read, 1986) with the graphics program TURBO-FRODO (Roussel and Cambillau, 1989). Successive rounds of rebuilding and simulated annealing refinements provided electron density maps that allowed complete interpretation of both the CDK2 and CksHs1 structures. X-PLOR omit maps from the final model were used to check every part of CDK2 and CksHs1 molecules systematically: ten and five residues of the structures of CDK2 and CksHs1, respectively, were deleted in each calculation, and simulated annealing was used to reduce model bias in omit maps. The final model (model B, described here), which matches the interface defined for crystal form A above, has an R factor of 19.8% for 11,938 reflections (all data) between 6 Å and 2.6 Å resolution and a free R factor of 29% (5%

of the reflections). This model comprises CDK2 residues Met-1 to Thr-39 and Thr-47 to Pro-294 and CksHs1 residues Gln-5 to Pro-74, with overall deviations from ideal geometry of 0.008 Å for bond distances and 1.5° for bond angles.

Because ATP and $MnCl_2$ interfere with the crystallization of the complex, the CDK2 catalytic active site is free and filled by solvent molecules. Of these, four are similarly positioned to the N1 and N7 atoms of the adenosine base, the O′2 atom of the ribose, and the γ-phosphate group of the ATP molecule bound to CDK2 (deBondt et al., 1993). Within the active site cleft, only the Phe-80 side chain flips conformation to interact with the Ala-31 side chain, compared with its homolog in the ATP-bound CDK2 structure. Temperature factors average 24 $Å^2$ for CDK2 main chain (N-lobe, 29 $Å^2$; C-lobe, 22 $Å^2$), 28 $Å^2$ for CksHs1 main chain, 26 $Å^2$ for CDK2 side chain (N-lobe, 32 $Å^2$; C-lobe, 24 $Å^2$), 31 $Å^2$ for CksHs1 side chain, and 28 $Å^2$ for 133 solvent molecules. High temperature factors and weak electron density occur for the CDK2 T loop (residues 152–163). The stereochemistry of the model was analyzed with PROCHECK (Laskowski et al., 1993), and 87% of the polypeptide backbone dihedral angles were found to lie in the most favored regions of the Ramachandran diagram, with the remainder in allowed regions. The coordinates of model B will be deposited with the Brookhaven Protein Data Bank.

Acknowledgments

We thank Carlos F. Barbas for access to his BIAcore instrument, Stephen Elledge for the two-hybrid plasmids, Henry Bellamy for access to beamline 1-5 at the Stanford Synchrotron Radiation Laboratory, and Brian R. Crane and Burley D. Phillips for help during data collection. We thank Sung-Hou Kim for the human CDK2 coordinates and Nikola P. Pavletich for the CDK2–cyclin A coordinates. Alicia Santiago kindly aided in constructing the *ckshs1* mutants, and Susan L. Bernstein purified the CksHs1 mutant proteins. M. H. W. was supported by the Medical Research Council of Canada. This work was supported in part by the Glaxo–Wellcome Research Institute.

Received January 9, 1996; revised February 15, 1996.

References

Arvai, A.S., Bourne, Y., Hickey, M.J., and Tainer, J.A. (1995a). Crystal structure of the human cell cycle protein CksHs1: single domain fold with similarity to kinase N-lobe domain. J. Mol. Biol. *249*, 835–842.

Arvai, A.S., Bourne, Y., Williams, D., Reed, S.I., and Tainer, J.A. (1995b). Crystallization and preliminary crystallographic study of human CksHs1: a cell cycle regulatory protein. Proteins *21*, 70–73.

Azzi, L., Meijer, L., Ostvold, A.-C., Lew, J., and Wang, J.H. (1994). Purification of a 15-kDa cdk4- and cdk5-binding protein. J. Biol. Chem. *269*, 13279–13288.

Bourne, Y., Arvai, A.S., Bernstein, S.L., Watson, M.H., Reed, S.I., Endicott, J.E., Noble, M.E., Johnson, L.N., and Tainer, J.A. (1995). Crystal structure of the cell cycle regulatory protein suc1 reveals a β-hinge conformational switch. Proc. Natl. Acad. Sci. USA. *92*, 10232–10236.

Bradford, M.M. (1976). A rapid and sensitive method for the quantitation of microgram quantities of protein utilizing the principle of protein-dye binding. Anal. Biochem. *72*, 248–254.

Brizuela, L., Draetta, G., and Beach, D. (1987). $p13^{suc1}$ acts in the fission yeast cell division cycle as a component of the $p34^{cdc2}$ protein kinase. EMBO J. *6*, 3507–3514.

Brünger, A.T., Kuriyan, J., and Karplus, M. (1987). Crystallographic R-factor refinement by molecular dynamics. Science *235*, 458–460.

Carson, P. (1991). RIBBONS 2.0. J. Appl. Cryst. *24*, 958–961.

Connolly, M.L. (1983). Solvent-accessible surfaces of proteins and nucleic acids. Science *221*, 709–713.

Cox, S., Radzio-Andzelm, E., and Taylor, S.S. (1994). Domain movements in protein kinases. Curr. Opin. Struct. Biol. *4*, 893–901.

deBondt, H.L., Rosenblatt, J., Jancarik, J., Jones, H.D., Morgan, D.O., and Kim, S.-H. (1993). Crystal structure of cyclin-dependent kinases 2. Nature *363*, 595–602.

Ducommun, B., Brambilla, P., and Draetta, G. (1991). Mutations at sites involved in suc1 binding inactivate cdc2. Mol. Cell. Biol. *11*, 6177–6184.

Dunphy, W.G. (1994). The decision to enter mitosis. Trends Cell Biol. *4*, 202–207.

Dunphy, W.G., and Newport, J.W. (1989). Fission yeast p13 blocks mitotic activation and tyrosine dephosphorylation of the Xenopus cdc2 protein kinase. Cell *58*, 181–191.

Durfee, T., Becherer, K., Chen, P.-L., Yeh, S.-H., Yang, Y., Kilburn, A.E., Lee, W.-H., and Elledge, S.J. (1993). The retinoblastoma protein associates with the protein phosphatase type 1 catalytic subunit. Genes Dev. *7*, 555–569.

Elble R. (1992). A simple and efficient procedure for transformation of yeasts. Biotechniques *13*, 18–20.

Endicott, J.A., and Nurse, P. (1995). The cell cycle and suc1: from structure to function? Structure *3*, 321–325.

Endicott, J.A., Noble, M.E., Garman, E.F., Brown, N., Rasmussen, B., Nurse, P., and Johnson L.N. (1995). The crystal structure of $p13^{suc1}$, a $p34^{cdc2}$-interacting cell cycle control protein. EMBO J. *14*, 1004–1014.

Fesquet, D., Labbe, J.C., Derancourt, J., Capony, J.P., Galas, S., Girard, F., Lorca, T., Shuttleworth, J., Doree, M., and Cavadore, J.C. (1993). The M015 gene encodes the catalytic subunit of a protein kinase that activates cdc2 and other cyclin-dependent kinases (CDKs) through phosphorylation of Thr161 and its homologues. EMBO J. *12*, 3111–3121.

Fisher, R.P., and Morgan, D.O. (1994). A novel cyclin associates with M015/CDK7 to form the CDK-activating kinase. Cell *78*, 713–724.

Goldsmith, E.J., and Cobb, M.H. (1994). Protein kinases. Curr. Opin. Struct. Biol. *4*, 833–840.

Gould, K.L., and Nurse, P. (1989). Tyrosine phosphorylation of the fission yeast cdc2+ protein kinase regulates entry into mitosis. Nature *342*, 39–45.

Hadwiger, J.A., Wittenberg, C., Mendenhall, M.D., and Reed, S.I. (1989). The *Saccharomyces cerevisiae* CKS1 gene, a homolog of the *Schizosaccharomyces pombe* suc1+ gene, encodes a subunit of the Cdc28 protein kinase complex. Mol. Cell. Biol. *9*, 2034–2041.

Hayles, J., Beach, D., Durkacz, B., and Nurse, P. (1986a). The fission yeast cell cycle control gene cdc2: isolation of a sequence suc1 that suppresses cdc2 mutant function. Mol. Gen. Genet. *202*, 291–293.

Hayles, J., Aves, S., and Nurse, P. (1986b). suc1 is an essential gene involved in both the cell cycle and growth in fission yeast. EMBO J. *5*, 3373–3379.

Hindley, J., Phear, G., Stein, M., and Beach, D. (1987). Suc1+ encodes a predicted 13-kilo-dalton protein that is essential for cell viability and is directly involved in the division cycle of *Schizosaccharomyces pombe*. Mol. Cell. Biol. *7*, 504–511.

Hu, S.-H., Parker, M.W., Lei, J.Y., Wilce, M.C.J., Benlan, G.M., and Kemp, B.E. (1994). Insights into autoregulation from the crystal structure of twitchin kinase. Nature *369*, 581–584.

Hunter, T. (1993). Braking the cycle. Cell *75*, 839–841.

Hunter, T., and Pines, J. (1994). Cyclins and cancer II: cyclin D and CDK inhibitors come of age. Cell *79*, 573–582.

Jeffrey, P.D., Russo, A.A., Polyak, K., Gibbs, E., Hurwitz, J., Massagué, J., and Pavletich, N.P. (1995). Mechanism of CDK activation revealed by the structure of a cyclinA-CDK2 complex. Nature *376*, 313–320.

Jessus, C., Ducommun, B., and Beach, D. (1990). Direct activation of cdc2 with phosphatase: identification of $p13^{suc1}$-sensitive and insensitive steps. FEBS Lett. *266*, 4–8.

Khatib, Z.A., Matsushime, H., Valentime, M., Shapiro, D.N., Sherr, C.J., and Look, A.T. (1993). Coamplification of the CDK4 gene with MDM2 and GLI in human sarcomas. Cancer Res. *53*, 5535–5541.

Knighton, D.R., Zheng, J., Ten Eyck, L.F., Ashford, V.A., Xuong, N.-H., Taylor, S.S., and Sowadski, J.M. (1991). Crystal structure of

the catalytic subunit of cyclic adenosine monophosphate-dependent protein kinase. Science *253*, 407–414.

Kusubata, M., Tokui, T., Matsuoka, Y., Okumura, E., Tachibana, K., Hisanaga, S., Kishimoto, T., Yasuda, H., Kamijo, M., Ohba, Y., Tsujimura, K., Yatani, R., and Inagaki, M. (1992). p13 suc1 suppresses the catalytic function of $p34^{cdc2}$ kinase for intermediate filament proteins, *in vivo*. J. Biol. Chem. *267*, 20937–20942.

Laskowski, R.A., MacArthur, M.W., Moss D.S., and Thornton, J.M. (1993). PROCHECK: a program to check the stereochemical quality of protein structures. J. Appl. Cryst. *26*, 283–291.

McGowan, C.H., and Russell, P. (1993). Human Wee1 kinase inhibits cell division by phosphorylating $p34^{cdc2}$ exclusively on Tyr15. EMBO J. *12*, 75–85.

Marcote, M.J., Knighton, D.R., Basi, G., Sowadski, J.M., Brambilla, P., Draetta, G., and Taylor, S.S. (1993). A three-dimensional model of the cdc2 protein kinase: localization of cyclin- and suc1-binding regions and phosphorylation sites. Mol. Cell. Biol. *13*, 5122–5131.

Meyerson, M., Enders, G.H., Wu, C.-L., Su, L.-K., Gorka, C., Nelson, C., Harlow, E., and Tsai, L.-H. (1992). A family of human cdc2-related protein kinases. EMBO J. *11*, 2909–2917.

Moreno, S., Hayles, J., and Nurse, P. (1989). Regulation of $p34^{cdc2}$ protein kinase during mitosis. Cell *58*, 361–372.

Morgan, D.O. (1995). Principles of CDK regulation. Nature *374*, 131–133.

Mueller, P.R., Coleman, T.R., Kumagai, A., and Dunphy, W.G. (1995). Myt1: a membrane-associated inhibitory kinase that phosphorylates cdc2 on both threonine-14 and tyrosine-15. Science *270*, 86–90.

Navaza, J. (1994). AMoRe: an automated package for molecular replacement. Acta Cryst. *A50*, 157–163.

Otwinowski, Z. (1993). Oscillation data reduction program. In Proceedings of the CCP4 Study Weekend, L. Sawyer, N. Isaacs, and S. Burley, eds. United Kingdom: SERC Daresbury Laboratory), pp. 56–62.

Parge, H.E., Arvai, A.S., Murtari, D.J., Reed, S.I., and Tainer, J.A. (1993). Human CksHs2 atomic structure: a role for its hexameric assembly in cell cycle control. Science *262*, 387–395.

Pines, J., and Hunter, T. (1991). Cyclin-dependent kinases: a new cell cycle motif? Trends Cell Biol. *1*, 117–121.

Poon, R.Y.C., and Hunter T. (1995). Dephosphorylation of Cdk2 Thr160 by the cyclin-dependent kinase-interacting phosphatase KAP in the absence of cyclin. Science *270*, 90–93.

Poon, R.Y., Yamashita, K., Adamczewski, J.P., Hunt, T., and Shuttleworth, J. (1993). The cdc2-related protein $p40^{MO15}$ is the catalytic subunit of a protein kinase that can activate $p33^{cdk2}$ or $p34^{cdk2}$. EMBO J. *12*, 3123–3132.

Read, R.J. (1986). Improved Fourier coefficients for maps using phase from partial structure with errors. Acta Cryst. *A42*, 140–149.

Reed, S.I. (1992). The role of p34 kinases in the G1 to S-phase transition. Annu. Rev. Cell Biol. *8*, 529–561.

Richardson, H.E., Stueland, C.S., Thomas, J., Russell, P., and Reed, S.I. (1990). Human cDNAs encoding homologs of the small p34 cdc28/cdc2-associated protein of *Saccharomyces cerevisiae* and *Schizosaccharomyces pombe*. Genes Dev. *4*, 1332–1344.

Rosenberg, A.H., Lade, B.N., Chui, D.S., Lin, S.W., Dunn, J.J., and Studier, F.W. (1987). Vectors for selective expression of cloned DNAs by T7 RNA polymerase. Gene *56*, 125–135.

Roussel, A., and Cambillau, C. (1989). TURBO-FRODO. In Graphics Geometry Partners Directory (Mountain View, California: Silicon Graphics).

Solomon, M.J. (1994). The function(s) of CAK, the $p34^{cdc2}$-activating kinase. Trends Biochem. Sci. *19*, 496–500.

Solomon, M.J., Harper, J.W., and Shuttleworth, J. (1993). CAK, the $p34^{cdc2}$ activating kinase, contains a protein identical or closely related to $p40^{MO15}$. EMBO J. *12*, 3133–3142.

Surana, U., Robitsch, H., Price, C., Shuster, T., Fitch, I., Futcher, A.B., and Nasmyth, K. (1991). The role of CDC28 and cyclins during mitosis in the budding yeast S. cerevisiae. Cell *65*, 145–161.

Tang, Y., and Reed, S.I. (1993). The Cdk-associated protein Cks1 functions both in G1 and G2 in *Saccharomyces cerevisiae*. Genes Dev. *7*, 822–832.

Taylor, S.S., and Radzio-Andzelm, E. (1994). Three protein kinase structures define a common motif. Structure *2*, 345–355.

Xu, R.-M., Carmel, G., Sweet, R.M., Kuret, J., and Cheng, X. (1995). Crystal structure of casein kinase-1, a phosphate-directed protein kinase. EMBO J. *14*, 1015–1023.

Zhang, F., Strand, A., Robbins, D., Cobb, M.H., and Goldsmith, E.J. (1994). Atomic structure of the MAP kinase ERK2 at 2.3 Å resolution. Nature. *367*, 704–711.